Natural Ventilation of a Tall Industrial Building: Investigation on the Impact of Modeling Assumptions

Ruijie Zhao[1,2] and Louis Gosselin[1,2]

1. Aluminium Research Centre-REGAL
2. Department of Mechanical Engineering, Université Laval, Québec City, Québec, Canada, G1V 0A6

Abstract

Aluminum potrooms are industrial buildings in which the smelting process releases large amounts of heat. In most of these tall buildings, ventilation relies solely on buoyancy and wind, and is critical to the process stability, workers' comfort and pollutants dispersion. A CFD model is currently being developed in order to determine the heat transfer, fluid flow and contaminant dispersion patterns under different scenarios, and as in every model, different simplifying assumptions are required. This paper studies the influence of some of the main modeling assumptions on the ventilation rate, such as the buoyancy model (e.g., Boussinesq versus incompressible ideal gas law), the boundary conditions, the reference density, etc. Simulations include both the interior and exterior of the building. Since the ultimate model will be multi-scale (i.e., three different, but coupled sub-models, (i) outdoor environment, (ii) potroom and (iii) smelting pots), a particular attention is devoted to the relation between these domains when analysing the results. Conclusions can be applied to the ventilation of different industrial buildings, as well as to other types of buildings.

1. Introduction

The Hall-Héroult process is dominantly used in modern primary aluminum production plants. A smelter contains a series of electrolytic cells, called pots, in each of which an electrical current circulates between a carbon anode and a cathode through an electrolytic bath in which alumina is dissolved. The carbon deoxidizes the alumina by a series of electro-chemical reactions, and as a result, carbon dioxide (CO_2) is emitted as a by-product. A liquid aluminum layer accumulates at the bottom of the pot and can be periodically siphoned. The overall process can be written in a very simplified and compact formula: $2Al_2O_3 + 3C + \text{electricity} \rightarrow 4Al + 3CO_2$. Although the process is a century old, the energy conversion efficiency is only about 50%, which means that roughly half of the input electricity is converted into heat. Since the process is very energy intensive, a tremendous amount of heat is dissipated into the potroom. A well designed potroom ventilation is required for cooling the room, removing fugitive emissions and maintaining acceptable working conditions. Modern potrooms are designed to achieve the right ventilation level using solely buoyancy forces. Heat is released from pots shell and increases the local air temperature, which creates a pressure difference between the exterior and interior of the potroom. A neutral plane establishes at a certain height where the indoor-to-outdoor pressure difference becomes zero. Under the neutral plane, the pressure difference pushes outside air into the potroom through the lower openings while above the neutral plane, the potroom air is evacuated to the

environment. The induced fresh air is distributed by several internal openings, e.g. the claustra wall (a brick wall with regularly arranged holes) on two lateral sides and the louvered openings on pot decks. This geometrical configuration forces the fresh air to sweep the sidewalls of each pot and provides an efficient cooling. The heated air rises up and escapes from the roof vent. A careful design should is necessary to provide enough ventilation where it is critical.

Computational Fluid Dynamics (CFD) has become a popular tool to study building ventilation during the last two decades, (Carrilho da Graça et al., 2002) (Zhai et al., 2007) (Liu et al., 2009) (Hussain and Oosthuizen, 2012). The computational domain usually includes an atmospheric environment outside the building in order to conveniently define boundary conditions. Although this method provides more accurate results, it requires large domain dimensions (between five and ten times those of the building itself), which requires a huge computational effort. However, when the detailed knowledge of the fluid flow and heat transfer patterns inside the building is focused, it becomes impractical to include both the exterior domain and a detailed interior geometry in terms of the number of discretized finite volumes. One strategy to cope with these difficulties is to cut off the domain at the building openings and apply "effective" boundary conditions at these openings. For example, Cook et al. (Cook et al., 2003) developed a CFD model for studying the natural ventilation of a single-storey enclosure and determined how to specify appropriate boundary conditions at the inlet and outlet of the enclosure. A good agreement was found between the CFD results and those from experiments. This method was further applied to a multi-storey building in (Ji and Cook, 2007).

In addition to the choice of the domain extent and boundary conditions, how the density is defined is also important in natural ventilation modeling. Boussinesq approximation is dominantly used for defining air density in the literature that was surveyed on CFD simulations of building ventilation. Few articles were found that simulate the air as an ideal gas. In addition, the wind-induced pressure should be well defined at the building openings of a model without the environment. Pressure coefficient on the exterior wall of building is required. They can be obtained by using primary methods such as direct measurements in a full scale building, wind tunnel measurements and CFD modeling. However, these methods are expensive and time consuming. Secondary methods, such as correlations or C_p (pressure coefficient) calculators, are available to obtain a quick estimate (Costola et al., 2009).

Compared with the available literature, the building studied in this paper (i.e., potroom) has some specificities. First of all, most of the literature considers commercial buildings and residences in which only moderate heat sources are present. In potrooms, the heat loss from the smelting pot surfaces to the potroom is usually as high as 5000 W/m^2. How to properly simulate the flow and heat transfer in such conditions is a challenge. Second, the geometry of the potroom has its own features that are quite different from commercial or residential buildings. Potroom can extend in length over 1000 m with width and height of only 20-30 m. In such a case, the approaching wind can basically blow over the building only from the roof side while, for normal buildings, the wind can reach the leeward side from both the roof and two lateral sides. Based on this point, the C_p on the exterior wall of such buildings should be investigated further. The

present work is a part of a larger project regarding potroom natural ventilation. Its scope is to develop a better knowledge of the impact of the modeling approaches and assumptions on this specific type of buildings, especially in terms of the modeling domain and the definition of the boundary conditions. In order to do that, we have tremendously simplified the geometry in the potroom. On the other hand, the inlet and outlet of the potroom are included in the models. Two potroom models, one with an environment and the other without it, were compared with each other under different scenarios. The model without the environment is estimated in terms of its capability to accurately simulate potroom ventilation compared to the more refined one. The objective is to find a proper procedure for modeling the aluminum smelting potroom without having to deal with the extra effort of modeling an outdoor environment.

2. Methodology and Description of CFD model

Physical model

Since having a knowledge of the flow pattern through building openings is of great importance to properly define boundary conditions, the first model (Model #1) includes both the interior and exterior of the potroom while the second model (Model #2) consists of only the potroom domain. Moreover, the internal geometry of the potroom was significantly simplified in the models, because in the present paper we are not interested into determining the exact airflow and heat transfer patterns, but rather to highlight the relative effect of the modeling options on ventilated mass flow rate, static pressure and temperatures, at the inlet and outlet of the potroom. The main model assumptions are listed below:

1. The potroom ventilation was simulated with a 2D model consisting of a sliced cross-section of the potroom. This appears to be a good simplification because the potroom length is quite long compared with the width and height. The width and height of the building are respectively W=28 m and H=22 m. For model #1, an outdoor atmosphere was created and the domain dimensions are dependent on the specifically studied scenario, as mentioned in the section "*Computational domain and grid*".
2. The detailed pot structure was mimicked by a simple pot profile and the flow path through the pot grilled openings is not simulated. Reminding the purpose of this work, accurate predictions of potroom ventilation and temperature profile are not necessary. A heat flux was defined on the pot surface to create a buoyancy force on the air in potroom. The heat flux was carefully chosen to yield reasonable results of potroom ventilation rate and air temperature at the roof vent.
3. The basement inlet and roof vent were created exactly as the real geometry.

Computational domain and grid

Because the simulations involve various environmental conditions, the computational domain was adapted to different scenarios. Figures 1a and 1b show the computational domains of model #1 when only buoyancy effect is taken into account (i.e., no wind) and when wind is present, respectively. In the former, the outdoor environment is extended 150 m from two lateral walls and the height of the top boundary is also 150 m. The domain becomes different in Fig. 1b, because it is created to simulate situations with

wind blowing from the left, in addition to the buoyancy driven flow. Based on the best practice guidelines by Franke et al. (Franke et al., 2011) and Tominaga et al. (Tominaga et al., 2008), the upstream domain is 10 times the building height (10H) and the downstream domain, 15H. The reason for a longer upstream domain will be explained in Section 4. The top boundary is set at a height of 10H in order to provide a small blockage ratio (10%). This ratio is a little larger than that recommended by the guidelines, because we should also notice that the simulated atmospheric boundary layer (ABL) does not extend far beyond the ground (H<200 m) where the assumption of constant shear stress is valid for defining the turbulent boundary conditions of the approaching wind (Richards and Hoxey, 1993). A higher ABL was also tested and little influence was found on the flow pattern around the building. The computational grids consisted of structured meshes and were created with the help of the pre-processor ICEM CFD 14.5. The distance of the center point of the first layer of near-wall control volumes to the wall is 0.05 m on all potroom walls where standard wall functions are used in the near-wall region. The mesh on pot surface is finer, with only 0.001 m between the wall and the center point of the first layer of control volumes. The reason for choosing this mesh is that the high heat flux imposed on the pot surface is basically the "engine" that drives the flow, and thus, the mesh should be fine enough to resolve the flow boundary layer in that zone. A growth ratio of 1.2 controls the cell growing from the building to the environmental boundaries. The computational domain of model #2 consists of only the

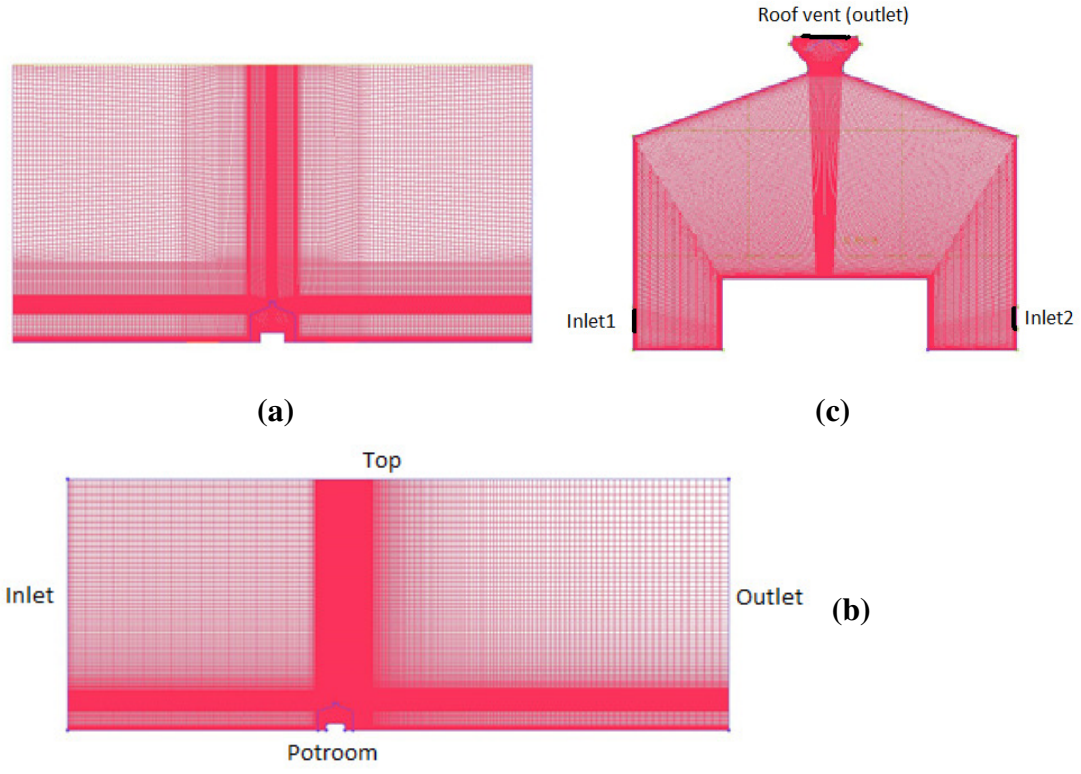

Figure 1: The computational domains and grids, (a) model #1, with buoyancy effect only; (b) model #1, with combined buoyancy and wind; (c) model #2, with only potroom

potroom, as shown in Fig. 1c. The grid was created following the same procedure as for model #1, except for a finer bulk grid in the potroom. In the end, the number of control volumes varied from 40 k to 100 k. Mesh independence was thoroughly investigated, but the details are not presented here.

A set of 3D computational domains was also made to study the dependence of the pressure coefficient on building geometry, which is of great importance for defining the wind-induced pressure in model #2. Fig. 2a shows a reference case where there is a small building standing in an approaching wind. The building in Fig. 2b represents a more realistic geometry of potroom. The building is extended from one lateral side of the environmental domain to the other side because a real potroom is extremely long. In such a situation, the approaching wind can reach the leeward side only from the roof. The influence of an extremely elongated building on the C_p values for the windward and leeward walls should be studied by comparing them with the reference case. Fig. 2c is a 2D model which is a projection of Fig. 2b in the plane perpendicular to the potroom length. The objective is to verify how well the 2D model can reproduce the simulated results. Detailed results are presented in Section 4. Grids were created as previously.

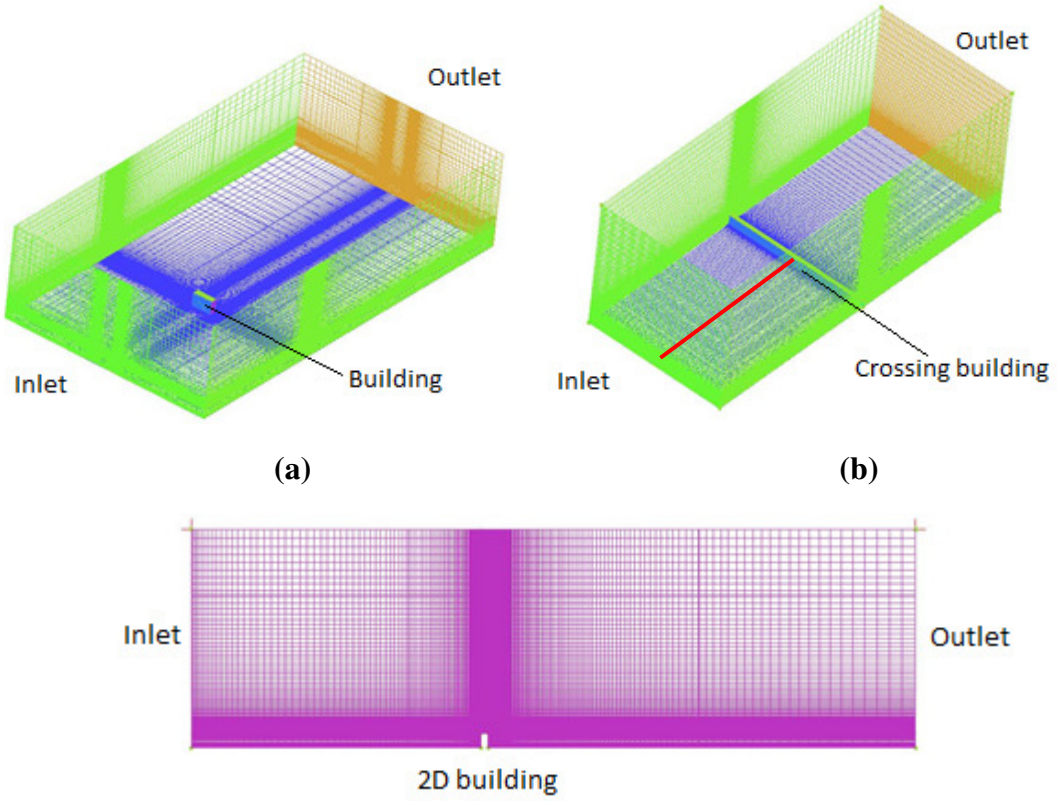

Figure 2: The computational domain and grids of the models for predicting C_p; (a) a "normal" building; (b) an elongated building; (c) 2D projection of the elongated building

Boundary conditions

In Fig. 1a, zero static pressure is applied at all environmental boundaries, since a purely buoyancy driven flow is simulated. The ambient temperature is 15℃ and the background radiation temperature is 1℃ based on the Mills correlation (Mills, 1999).

In Fig. 1b, where a wind comes from the left side, the inlet boundary conditions (i.e. mean velocity U, turbulent kinetic energy k and turbulence dissipation rate ε) are defined based on the equations proposed in Ref. (Richards and Hoxey, 1993). The sand-grain roughness height k_s is 0.1 m and the roughness constant C_s is set as 1. Zero static pressure is defined at the outlet, i.e. the right side of the domain. Symmetry is applied at the top, where there is zero normal velocity and zero normal gradients of other variables. Thermal and radiative parameters are the same as in Fig. 1a.

In Fig. 1c, the potroom inlet area is reduced by multiplying the real dimension by a factor 0.61, to take into account the vena contracta phenomenon at the inlet. The static pressure at the inlet and outlet, if there is a wind outside, are calculated based on the Cp value and the wind speed. Note that Cp is obtained from either the simulation with model #1 or a Cp generator software (Costola et al., 2009). Both convection and radiation between the potroom walls and the outdoor environment are considered. The correlations in (Defraeye et al., 2011) are used to calculate the convective heat transfer coefficients on windward and leeward surfaces and the correlation in (Mills, 1999) is used for calculating the radiation exchange with sky. Solar radiation was not taken into account in the present models.

As for the simulations of Fig. 2a-c, the boundary conditions are defined as in Fig. 1b, except that the air is assumed to be isothermal (energy equation is not solved).

Solver settings and mesh independence study

The equations that express the conservations of mass, momentum and energy in the modeling domain were solved in ANSYS FLUENT 14.5 via the finite volume method. Turbulence was modeled by using the Realizable k-ε model, which is a most recent model in the family of k-ε models. When using model #1, the pseudo transient simulation was performed because it gave a faster convergence than a steady-state calculation. Convergence was declared only when the monitored parameters were not changing between consecutive iterations (the scaled residuals of mass, momentum and energy can reduce to very small values, e.g. $<10^{-12}$).

Transient simulation was used in model #2, because of the difficulty to achieve convergence in steady-state calculations. A small time step of 0.2 s was used at the beginning of the simulation and was progressively increased during the simulation. The convergence for each time step was declared when the scaled residuals reached 10^{-5} for continuity, momentum, k and ε and 10^{-8} for energy. In all simulations, pressure interpolation was realized with PRESTO! and second-order upwind schemes were used for other terms in the equations.

A mesh independence study was performed by comparing two grids, the current grid and a finer grid. The current grid has 41.3k cells while the finer grid has 114.3k cells in

model #1. The relative difference in the prediction of mass flow rate through the potroom vent is only 0.2% and that of the air temperature at vent is 0.4%. The average temperature discrepancy on pot surface between the two grids is 0.3℃ and the predicted heat transfer by convection on pot surface has a relative difference of 0.8%. Therefore, the proposed grid is considered fine enough for the studied cases.

3. Natural ventilation with buoyancy driven flow only

Effect of the density definition in model #1

Boussinesq approximation is widely used in CFD simulations involving heat transfer in buildings. It assumes that the air density change has a linear relationship with the temperature change, and that density variations are very small compared to the density value (i.e. $\Delta\rho / \rho \approx \beta(T - T_\infty) \ll 1$). This simplification is efficient and valid when the temperature difference is limited, which is suitable for many simulations of building environments. However, in a smelter, the temperature on pot surfaces is quite high and the temperature difference near pot shell could be as high as 300℃ ($\beta(T - T_\infty)$ could reach 0.6~0.7). Therefore, the validity of the Boussinesq approximation can be questionable. Two other ways to take into account the variations of density with temperature (i.e., state functions) were also considered, and are described below.

ANSYS FLUENT 14.5 provides an incompressible ideal gas law to determine the air density:

$$\rho = \frac{p_{op}}{\frac{R}{M_w}T} \tag{1}$$

where R is the universal gas constant, M_w, the molecular weight of the gas, T, the temperature and p_{op}, the defined operating pressure. p_{op} is a constant pressure, normally representing a mean pressure in the computational domain. In the CFD models of this work, the pressure at the middle height of the simulated domain was considered as p_{op}. In Eq. (1), the local density field depends only on the local temperature field. It should be mentioned that a reference density ρ_{ref} is also required in FLUENT to define a "reduced pressure" $p' = p - \rho_{ref} gh$. In this definition, the hydrostatic pressure is automatically included in the pressure term as $\rho_{ref} gh$.

We also defined the air density based on the ideal gas law in FLUENT:

$$\rho = \frac{p_{op} + p'}{\frac{R}{M_w}T} \tag{2}$$

where p' is the local relative pressure predicted by FLUENT. The reference density here is set to 0, because the hydrostatic pressure has to be calculated in the equations. Now, the sum of p_{op} and p' is the absolute pressure and the density is determined by both local pressure and temperature.

In model #1 with only buoyancy (no wind), the three different approaches to consider density variations (i.e., Boussinesq approximation, incompressible ideal gas law and ideal gas law) were compared. Table 1 reports the impact of the state function on some of the important simulation results. It is found that the discrepancies are very small between the incompressible ideal gas law and the ideal gas law. However, the Boussinesq approximation overestimated the mass flow rate through the roof vent and the heat transfer by convection on pot surfaces, compared with the other methods. The predicted average temperature on pot surface with the Boussinesq approximation is approximately 10℃ below that with the two other methods. The Boussinesq approximation also overestimates the convective heat transfer around pot surface. The ideal gas law is the most accurate way to calculate the air density, but the incompressible ideal gas law has shown to provide similar results. Since the latter is easily available in FLUENT and convenient to apply, it was chosen for the rest of the simulations.

Table 1: Comparisons of the CFD results as a function of the method to determine how air density is defined

	Boussinesq approximation	Incompressible ideal gas law	Ideal gas law
$\dot{m}$ at roof vent (kg/s)	3.00	2.76	2.77
T_a at roof vent (℃)	35.1	34.7	36.1
T_{ave} on pot surface (℃)	251.9	262.7	262.6
Heat transfer by convection on pot surface (kW)	49.2	42.1	42.3

Comparison of the predictions of potroom ventilation between models #1 and #2

One of the main objectives of this work is to verify the possibility of modeling the potroom ventilation by using a model similar to #2, i.e. only with the interior of the potroom. Therefore, the results obtained from two models were compared in order to determine proper modeling settings for model #2. Incompressible ideal gas law was used in both models. The choice of the reference density, used in defining reduced pressure, is a challenge for obtaining an accurate result from model #2, because the exact pressure at the inlet and outlet is unknown. Here, the density at the ambient temperature 15℃ was chosen as the reference density and zero static pressure was applied at the inlet and outlet. The comparison is reported in Table 2. With this approach, the two models (i.e., with or without the domain exterior to the potroom) show a good agreement in predicting the most interesting parameters. The definition of the boundary conditions of model #2 is adequate to obtain reliable results. Another simulation was performed with model #2 where we defined the static pressure calculated from model #1. This test case is named model #2 with adaptive pressure at inlet and outlet in Table 2. However, the predicted mass flow rate at roof vent is smaller than that in the previous model. This emphasizes again that the procedure to deal with the boundary condition (i.e. downscaling the inlet, reference density the same as the outdoor air density and zero static pressure at boundaries) is correct in model #2.

Table 2: Comparison of the results of potroom ventilation between models #1 and #2 (i.e., with or without domain outside the potroom)

	Model #1	Model #2	Model #2 with adaptive pressure at inlet and outlet
$\dot{m}$ at roof vent (kg/s)	2.76	2.82	2.54
T_a at roof vent (℃)	34.7	33.2	35
T_{ave} on pot surface (℃)	262.7	262.1	262.4
Heat transfer by convection on pot surface (kW)	42.1	41.5	41.4

Impact of ambient temperature

The modeling methods were further challenged for three different ambient temperatures: −10℃, 15℃ and 35℃, representing the ambient temperature in different seasons. The results of the two models were compared and the coherence was maintained at different ambient temperatures. An interesting finding is that the ventilated air flow rate at the roof vent could vary significantly when the ambient temperature is changed. For example, the predicted mass flow rate is increased by 30% when the ambient temperature reduces from 35℃ to −10℃. This is reasonable as the ambient temperature influences the reference density and eventually changes the pressure difference across the inlet and outlet. A significant increase of potroom ventilation in cold ambient conditions also explains why smelters need to close the inlets of potroom by using panels during the winter season, in order to limit the amount of cold air into the potroom and keep it comfortable for the operators.

4. Impacts of wind

In a real situation, the ventilation in potroom is usually a consequence of the combination of buoyancy and wind-driven forces. Therefore, a good prediction of the wind-induced pressure is crucial for the simulation of potroom ventilation when model #2 is used. In this section, we first validate the capability of the CFD model (model #1) to successfully predict the pressure coefficient C_p on the exterior walls of potroom in an isothermal atmosphere. Then, a scenario combining buoyancy and wind driven forces is investigated and the results are compared with those obtained with the potroom model (model #2). The objective is to verify the capability of model #2 to simulate the potroom ventilation in windy conditions.

Impact of building geometry

As shown in Fig. 2, different building geometries were studied in windy conditions. A reference wind speed was chosen as 7 m/s at the building height (10 m) and the flow was considered isothermal in a standard condition, i.e. air density ρ=1.225 kg/m^3. We only considered a wind approaching from the direction perpendicular to the windward wall, because a 2D model cannot simulate any other direction. The dependence of C_p on the wind direction could be determined in a future work by using a 3D model for studying the potroom ventilation. Figs. 3a and 3b show the distribution of C_p on windward and leeward surfaces of the reference case. A good agreement is found

between the predictions and up-to-date literature (Montazeri and Blocken, 2012) (ASHRAE, 2009), which validates the prediction and accuracy of the model. Then, the model of Fig. 2b was simulated in the same wind condition. Fig. 3c (blue symbols) shows the C_p on this building. It exhibits significant differences in both values and distributions compared to the C_p on the reference building. The maximum C_p on the windward surface is only 0.5 while it is usually in the range 0.7-0.8 in the buildings studied in the referred literature. On the leeward side, the minimum C_p reaches −1, compared with more conventional value around −0.5. Meanwhile, the variation of C_p happens only in the vertical direction (which is why we reported the results as in Fig. 3c). All observations reveal that the wind-induced pressure could be quite different on an extremely long building. The approaching wind can only access to the leeward side from the roof as the building is regarded as infinite along the width of the computational domain. The lack of access for wind moving over the building can prevent the pressure recovery in the wake area behind the building. A larger negative pressure on the leeward surface is expected. Because of the assumption of an infinitely long building, no wind can move from the lateral side and C_p will be constant in the horizontal direction. A 2D model was created to simplify the simulation model. Fig. 3c (red symbols) reports the C_p distribution on windward and leeward surfaces of the 2D building. A good agreement between the two

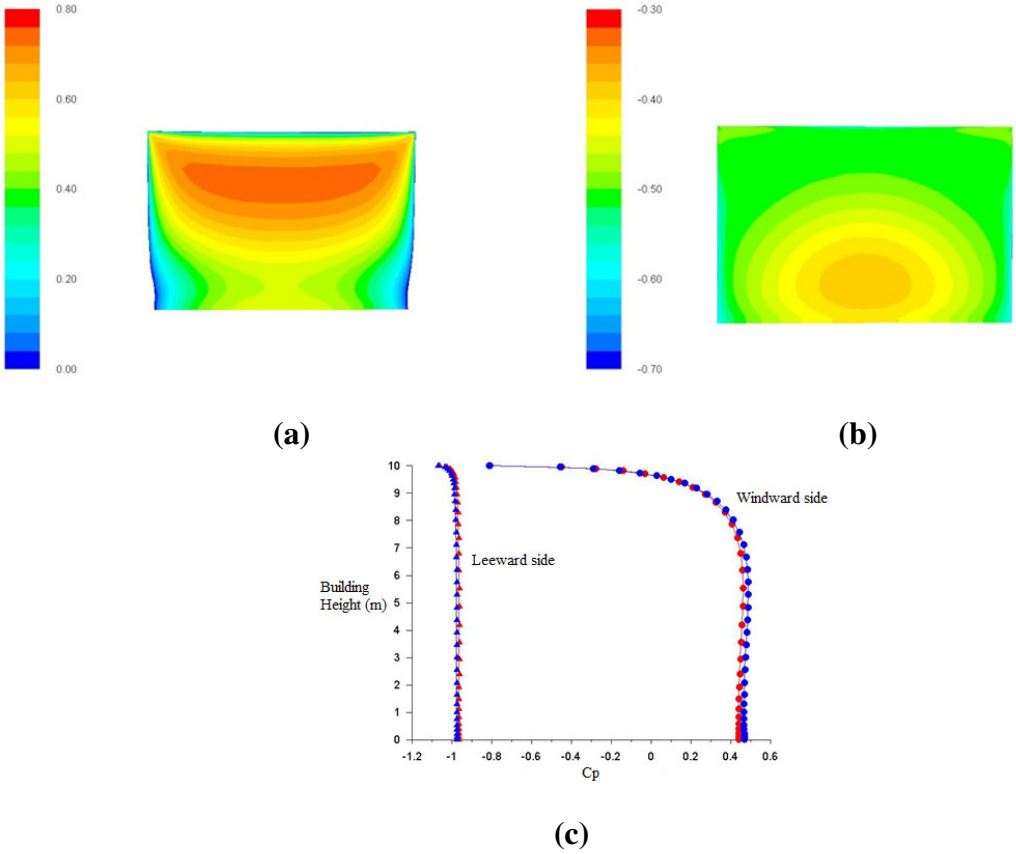

Figure 3: C_p distribution on (a) windward surface of building in Fig. 2a, (b) leeward surface of building in Fig. 2a; (c) C_p distribution on the building in Fig. 2b, circles indicate windward side and triangles, leeward side, blue symbols are the results from the 3D building in Fig. 2b and red symbols, from the 2D building in Fig. 2c

models indicates that 2D model can reproduce the wind induced pressure calculated with a 3D model when the wind is perpendicular to the wall.

A particular attention is devoted to the definition of the reference static pressure. The C_p values are calculated as $C_p = (P - P_{ref})/(0.5\rho U^2_{ref})$ where P is the pressure at wall, P_{ref} the reference static pressure, ρ the environmental air density and U_{ref} the reference wind speed at building height. Normally, the reference static pressure is the free stream pressure in the upstream wind where the presence of building has no influence on the flow field. This value is not easy to be accurately determined. We created a line at the roof height and in the middle of the domain, as depicted by a red line in Fig. 2b. Along this line, the wind velocity component in x (aligned with the wind direction) and the static pressure can be determined from the simulation. We defined the reference pressure as the flow static pressure at the position where the wind velocity component in x is reduced by 10 %. In the area between this point and the windward wall, the flow field is significantly influenced by the building.

Comparison of the predictions of potroom ventilation between models #1 and #2

Since the reliability of the C_p prediction was proved in the above section, we used the model in Fig. 1b to study the potroom ventilation in windy conditions. The simulations were performed with wind speeds of 10 km/h and 20 km/h, respectively. Note that the wind speed here refers to the reference speed at a 10 m height. The temperature and radiation were included in the simulations. The first comparison was made in terms of the predicted C_p at the inlet and roof vent in two cases: one with isothermal air, and the other with a heat flux imposed on the pot surface, as listed in Table 3. In the former case, the windward average C_p is 0.57 and the leeward C_p is -1.3. These values are very close to the situation studied in the previous section. Once heat is introduced to the model in the second case, the predicted C_p becomes 0.6 on the windward wall and −2 on leeward. Note that the C_p in this case is actually an "effective pressure coefficient" considering both buoyancy and wind force. A significant increase is found in the C_p of leeward. Fig. 4 shows the temperature profile in the domain. We can see that a portion of heated air comes out from the inlet of the leeward side. This is because the internal potroom geometry is simplified and cross over ventilation is easily achieved (which is not necessarily the case in current potroom geometry). Another reason is that the heated air exiting from the inlet will rise up due to buoyancy and further reduce the pressure there. This phenomenon illustrates that the C_p data which only considers the wind induced pressure will not be sufficient when a cross over ventilation occurs between the two inlets at the bottom. In a real potroom, some components (e.g. perforated walls at two lateral sides, the pot body and its auxiliary parts) are present, and thus, the cross over ventilation is more difficult to be realised (air is typically moving out from the roof vent).

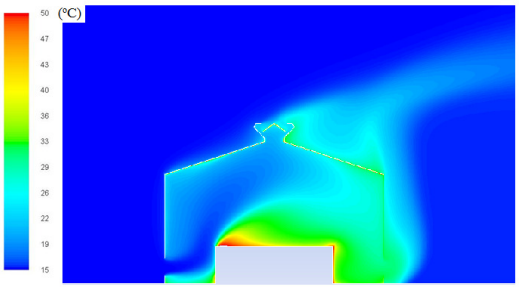

Figure 4: The air temperature profile with a 10 km/h wind speed

Next, we studied how well model #2 could accurately predict the ventilation in windy conditions. The C_p data were adopted from two sources: the software "C_p generator" and model #1. C_p generator is developed by TNO, an independent research organization in the Netherlands. It predicts the dimensionless static wind pressure coefficients on the façades and roofs of block-shaped buildings, with or without pitched roofs. It accounts for wind shielding by neighboring buildings and terrain roughness. The predictions of the software are also reported in Table 3. It is found that there are significant deviations compared to the values predicted by CFD models. In fact, they are more similar to the C_p on a conventional building. The reason for the discrepancy can come from the fact that C_p generator was not originally designed for buildings with the features of a potroom.

The C_p data calculated from model #1 were adopted to define the pressure at the boundaries of model #2. Both isothermal and thermal cases were tested in model #2. In a conventional approach, C_p takes into account only the wind induced pressure on the building façades. However, when using the C_p data from the isothermal case, the model #2 overestimated the ventilated mass flow rate at roof vent by 33%, compared with that of model #1. This is because the C_p on the leeward wall is only -1.32 in an isothermal case while it is -2.0 in a "thermal" case. A smaller negative pressure at the leeward wall makes more air exiting from the roof vent. Then, the C_p values obtained from the "thermal" case or the "effective pressure coefficients" were adopted in model #2 and it is found that the predicted mass flow rate at roof vent has only 2% relative difference with model #1. This thermal effect induces little change on the C_p at the roof vent in terms of the simulation results of model #1 and about -1.2 was observed in both isothermal and thermal conditions. The results have revealed that it can be a challenge to properly define the pressure imposed by the outside wind for potroom, especially for the openings at the leeward side. When there is strong cross over ventilation occurring between the inlets, the exited hot air could significantly influence the pressure at the leeward side. If the ventilation rate is the main interest of the simulations, a model with only the potroom domain might not be sufficient to provide accurate results, especially in a situation with a strong wind influence.

Table 3: C_p data adopted from different sources

Position	Model #1_isothermal	Model #1_heat	C_p generator
Windward inlet	0.57	0.6	1.2
Leeward inlet	-1.32	-2.0	-0.5
Roof vent	-1.0	-0.9	-1.3

5. Conclusions

This paper presents a systematic analysis of the modeling of natural ventilation in an aluminum smelting potroom. The main features that differentiate such a building are its shape, its internal gains, and its large (natural) ventilation rate. The effects of pure buoyancy and the combination of buoyancy and wind were investigated in CFD simulations. The ventilated mass flow rate at the roof vent was predicted in the computational domain with and without an outdoor environment. The purpose is to evaluate the capability of the model without an outdoor environment in modeling the natural ventilation in potrooms. The results achieved for different scenarios provide us with an in-depth insight on modeling the natural ventilation in potrooms. The results have indicated that the incompressible ideal gas law is more desirable in the definition of air density, because there is a large temperature difference in the area near the pot surface. The model without the simulation of the outdoor environment (model #2) can predict accurate heat transfer and flow patterns in the building in situations where buoyancy dominates. A special attention should be devoted to the choice of the reference density which is used to consider the hydrostatic pressure. In the model #2, this density is determined based on the temperature of the outdoor environment rather than the mean temperature in the computational domain which is usually the default setting in FLUENT. Model #2 was not accurate in predicting potroom ventilation by using C_p data calculated from correlations or C_p calculators which were developed based on studies on conventional buildings. In fact, the simulations of the C_p on the potroom faces have revealed a different value and distribution, compared with that on normal buildings. Moreover, the pressure on leeward surface could also be influenced by the ventilated hot air if a cross over ventilation occurs between the two inlets. The simulation of outdoor environment seems to be necessary for a good prediction of potroom ventilation in windy conditions, because of the challenge of providing a good prescribed C_p.

In reality, there are always some neighbor buildings around a potroom (e.g. other potrooms, gas treatment center, office buildings, anode plant). This will likely reduce local wind speed compared to that measured at a meteorological tower. Since the wind dynamic pressure is proportional to the square of the velocity, the reduction will significantly diminish the wind induced pressure at the inlet and outlet of potrooms. The model without environment could thus be sufficient to simulate the ventilation in weak wind during most time of a year. Further research could focus on this aspect. The results of this paper will be used in the development of a more realistic, integrated and advanced potroom ventilation model.

Acknowledgements

This work is supported by the Chinese Scholarship Council (CSC). The authors also acknowledge the support from Fonds de recherche du Québec – Nature et Technologies (FRQNT) and from REGAL-Aluminum Research Centre. The authors would like to thank Alcoa for its active involvement in this project.

References

ASHRAE, 2009. ASHRAE Handbook–Fundamentals. Atlanta GA 24.3–24.5.

Carrilho da Graça, G., Chen, Q., Glicksman, L.R., Norford, L.K., 2002. Simulation of wind-driven ventilative cooling systems for an apartment building in Beijing and Shanghai. Energy Build. 34, 1–11.

Cook, M.J., Ji, Y., Hunt, G.R., 2003. CFD modelling of natural ventilation: combined wind and buoyancy forces. Int. J. Vent. 1, 169–179.

Costola, D., Blocken, B., Hensen, J.L.M., 2009. Overview of pressure coefficient data in building energy simulation and airflow network programs. Build. Environ. 44, 2027–2036.

Defraeye, T., Blocken, B., Carmeliet, J., 2011. Convective heat transfer coefficients for exterior building surfaces: Existing correlations and CFD modelling. Energy Convers. Manag. 52, 512–522.

Franke, J., Hellsten, A., Schlunzen, K.H., Carissimo, B., 2011. The COST 732 Best Practice Guideline for CFD simulation of flows in the urban environment: a summary. Int. J. Environ. Pollut. 44, 419–427.

Hussain, S., Oosthuizen, P.H., 2012. Numerical investigations of buoyancy-driven natural ventilation in a simple atrium building and its effect on the thermal comfort conditions. Appl. Therm. Eng. 40, 358–372.

Ji, Y., Cook, M.J., 2007. Numerical studies of displacement natural ventilation in multi-storey buildings connected to an atrium. Build. Serv. Eng. Res. Technol. 28, 207–222.

Liu, P.-C., Lin, H.-T., Chou, J.-H., 2009. Evaluation of buoyancy-driven ventilation in atrium buildings using computational fluid dynamics and reduced-scale air model. Build. Environ. 44, 1970–1979.

Mills, A.F., 1999. Heat Transfer, 2nd edition. ed. Prentice Hall, New Jersey.

Montazeri, H., Blocken, B., 2012. CFD simulation of wind-induced pressure coefficients on buildings with and without balconies: validation and sensitivity analysis. Build. Environ.

Richards, P.J., Hoxey, R.P., 1993. Appropriate boundary conditions for computational wind engineering models using the k-ϵ turbulence model. J. Wind Eng. Ind. Aerodyn. 46, 145–153.

Tominaga, Y., Mochida, A., Yoshie, R., Kataoka, H., Nozu, T., Yoshikawa, M., Shirasawa, T., 2008. AIJ guidelines for practical applications of CFD to pedestrian wind environment around buildings. J. Wind Eng. Ind. Aerodyn. 96, 1749–1761.

Zhai, Z.J., Zhang, Z., Zhang, W., Chen, Q.Y., 2007. Evaluation of various turbulence models in predicting airflow and turbulence in enclosed environments by CFD: Part 1—Summary of prevalent turbulence models. HvacR Res. 13, 853–870.